Chemical control of orbital polarization in artificially structured transition-metal oxides: La$_2$NiXO$_6$ (X=B, Al, Ga, In) from first principles

M. J. Han,[1] C. A. Marianetti,[2] and A. J. Millis[1]

[1]*Department of Physics, Columbia University, New York, New York 10027, USA*

[2]*Department of Applied Physics, Columbia University, New York, New York 10027, USA*

The application of modern layer-by-layer growth techniques to transition-metal oxide materials raises the possibility of creating new classes of materials with rationally designed correlated electron properties. An important step toward this goal is the demonstration that electronic structure can be controlled by atomic composition. In compounds with partially occupied transition-metal d shells, one important aspect of the electronic structure is the relative occupancy of different d orbitals. Previous work has established that strain and quantum confinement can be used to influence orbital occupancy. In this paper we demonstrate a different modality for orbital control in transition-metal oxide heterostructures, using density-functional band calculations supplemented by a tight-binding analysis to show that the choice of nontransition-metal counterion X in transition-metal oxide heterostructures composed of alternating LaNiO$_3$ and LaXO$_3$ units strongly affects orbital occupancy, changing the magnitude and in some cases the sign of the orbital polarization.

I. INTRODUCTION

Recent progress in growth of transition-metal oxide multilayers with atomic-scale chemical precision[1] suggests that it may become possible to create new classes of materials with desirable electronic properties based on aspects of correlated electron physics such as high Curie temperature ferromagnetism,[2,3] "colossal" magnetoresistance,[4] correlation-driven metal-insulator transitions,[5] and high transition temperature superconductivity.[6] The ultimate goal is "materials by design," in other words to construct systems with desired electronic properties. A necessary first step is to design and fabricate systems with a desired electronic structure.

The "correlated electron" properties of transition-metal oxides are controlled in part by the relative occupancy of the different transition-metal d orbitals.[7] Controlling the orbital occupancy by materials design is therefore an important milestone in the progress toward a rational design of correlated electron materials. A difference in relative occupancies of orbital states may be described as an "orbital polarization" in analogy to the difference in occupancies of spin states which gives rise to spin polarization. As the control of spin polarization is achieved by application of appropriate magnetic fields, so the control of orbital polarization may be achieved by identification and manipulation of appropriate "orbital fields."

Two classes of "orbital field" are well established: strain and quantum confinement. Lattice strain works because in a transition-metal oxide the hybridization between the transition-metal d orbital and the oxygen p states produces ligand fields whose strength depends on the geometrical distance between the transition metal and oxygen site. An applied strain changes relative bond lengths, thereby affecting the ligand fields. Strain control was reported by Konishi *et al.*,[8] who grew films of "colossal magnetoresistance" manganites on substrates which imparted compressive, negligible, or tensile strain to the manganite film. The systems exhibited

resistivities which were, respectively, strongly insulating, weakly insulating, and metallic and the change in resistance was attributed to a strain-induced change in relative occupancies of the $d_{x^2-y^2}$ and $d_{3z^2-r^2}$ orbitals on the electrically active Mn site.

The quantum confinement effect works because each transition-metal d orbital has a specific spatial structure which leads to a direction-dependent hopping amplitude. Spatially anisotropic quantum confinement (for example, in a heterostructure composed of alternating transition-metal oxide and insulating spacer layers) allows electrons to delocalize more in some directions than in others, thereby allowing some orbitals to gain more delocalization energy than others. The quantum confinement effect operates in a slightly subtle way in transition-metal oxide systems, where the relevant electronic bands are antibonding combinations of transition-metal d and oxygen p states. In the single-crystal form of many transition-metal oxide materials the transition-metal-oxygen hybridization vanishes at the zone center (Γ) point of the Brillouin zone. The bands are degenerate or nearly degenerate at this point and disperse upward from it. A partial breaking of translational symmetry activates the hopping at zone center, thus lifting some orbitals up relative to others. Chaloupka and Khalliulin[9] recently proposed that in a heterostructure composed of alternating layers of LaNiO$_3$ (LNO) and LaAlO$_3$ this effect could lead to a situation in which only the x^2-y^2 Ni e_g symmetry orbital would be occupied, providing an electronic structure similar to that found in high-T_c copper-oxide superconductors. The issue was studied theoretically by Hansmann *et al.*[10]

In this paper we identify a third route to control of orbital polarization based on chemical composition of spacer layers in an oxide superlattice. We consider specifically the class of systems introduced by Chaloupka and Khaliullin,[9] namely, superlattices composed of alternating layers of LaNiO$_3$ and of a spacer layer LaXO$_3$ the orbital polarization depends upon the choice of counterion X, even when X is chosen such that LaXO$_3$ is a wide-band-gap insulator. In this situation the
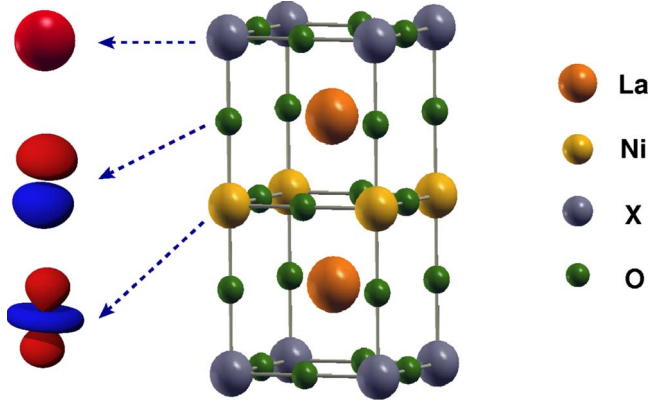
FIG. 1. (Color online) Central portion: unit cell of (001) super-lattice considered in this paper with atoms indicated on right. Left side: chain of hybridizing orbitals (top to bottom X_s, O_{p_z}, and $Ni_{3z^2-r^2}$) controlling relative occupancy of $d_{3z^2-r^2}$ orbital.

conventional wisdom is that because the LaXO$_3$ layers are insulating, the only relevant effects are strains induced by lattice mismatch between the LaNiO$_3$ and the LaXO$_3$ layers. We show that this is not the case, and that the strength of chemical bonding of the apical oxygen with the X ion significantly affects the polarization, even changing its sign in some cases.

The rest of this paper is organized as follows. Section II presents the systems we study, the definitions we use and the formalism we apply. Section III presents the band structures and resulting orbital polarizations in the simple case where lattice relaxations are forbidden. Section IV presents a tight-binding (TB) analysis which explicates the physics behind the results presented in Sec. III. Section V considers the additional effects of lattice relaxation. Section VI is a summary and conclusion.

II. MODEL, DEFINITIONS, AND METHODS

We consider superlattices of the form depicted in Fig. 1 composed of blocks of LaNiO$_3$ and another material LaXO$_3$, alternating along the (0001) axis of the basic perovskite crystal structure. We choose X=B, Al, Ga, and In from column 3A of the periodic table. While to our knowledge only LaAlO$_3$ has been used to grow oxide superlattices, all of the LaXO$_3$ compounds have been reported in the literature.[9,11,12] For simplicity we take all Ni-O-Ni and Ni-O-X-O-Ni bonds angles to be 180°. In most of our calculations we fix the in-plane lattice constants to the generalized gradient approximation (GGA)-optimized pseudocubic bulk LaNiO$_3$ value 3.81 Å but in some of our calculations the in-plane lattice constant was set to 3.91 Å to model the effect of a film grown on an SrTiO$_3$ (STO) substrate. We consider two cases, an "unrelaxed" case where the out-of-plane lattice constant is set equal to the in-plane one, and a "relaxed" structure where the out-of-plane atomic positions are adjusted to minimize the energy as described below.

To determine the electronic structure we use density-functional band theory within the GGA as implemented in the Vienna *ab initio* simulation package (VASP).[13–16] We used
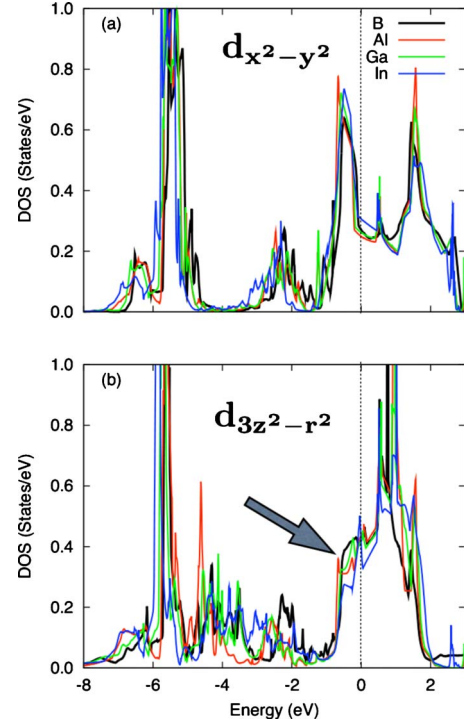

FIG. 2. (Color online) d-projected density of states (upper panel x^2-y^2; lower panel $3z^2-r^2$) of (001) La$_2$NiXO$_6$ heterostructures with counterlayer B-site ion X=B (black), Al (red), Ga (green), and In (blue), obtained from GGA band-theory calculations for unrelaxed structure [ideal cubic perovskite, doubled in (001) direction] with all Ni-O and X-O bond lengths taken to be one half of the bulk LaNiO$_3$ lattice parameter a=3.81 Å. Arrow in lower panel indicates region where dependence of $d_{3z^2-r^2}$ density of states on counterion is evident.

a plane-wave basis set and the projector augmented wave method[17] with a cutoff of 270 eV and k-point meshes of $10\times10\times5$. In the relaxed calculations, atomic positions were relaxed along the (001) using conjugate gradient minimization of the GGA energy.

To determine orbital occupancies we projected the calculated electronic density of states onto locally defined atomic orbitals obtained by defining a sphere around the atom in question and then projecting the wave functions within the sphere onto the appropriate symmetry states. The sphere sizes in angstrom were taken to be 1.286(Ni d)0.820(O p) (these are the VASP defaults) while for the X s orbital on all of the counterions we used 1.402.

Examples of our results for d-projected densities of states are shown in Fig. 2. The density of states consists of two components: a broad antibonding band (of mixed Ni d/O p character) spanning the region from ~-1.5 to ~2 eV near the chemical potential and a narrow bonding band at the low energy $E\sim-6$ eV. As can clearly be seen, the lower edge of the Ni-O antibonding band is well defined. Orbital occupancies are then obtained from integrals of the densities of states; representative results are shown in Fig. 3. That the integrals are not numerically equal to 2 is related to the sphere size. We are interested in the occupancies $n_{x^2-y^2}$ and $n_{3z^2-r^2}$ of the near Fermi-level d-p antibonding bands. To
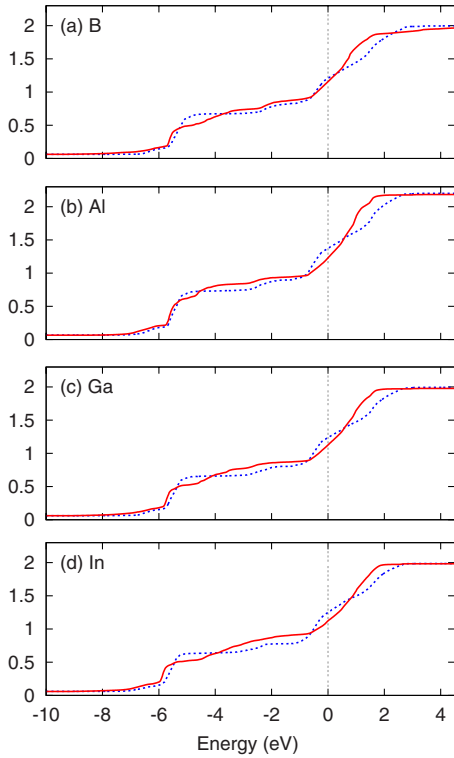
FIG. 3. (Color online) Integral of Ni $d_{3z^2-r^2}$ (red solid line) and Ni $d_{x^2-y^2}$ (blue dashed line) density of states for the four choices of X ion considered in the paper. Flat region between ~-2 and ~-1 eV defines lower edge of conduction band.

obtain these we take the difference between the value of the density of states integral at the lower edge of the antibonding band (identified from the flat part of the integrated density of states plot) and the value at the Fermi level. Values corresponding to integrating over the entire conduction-band plots of integrated d spectral weight vs energy may be read directly from Fig. 3 and yield the same conclusions.

From the orbital occupancies we obtain the orbital polarization P which we define as

$$P = \frac{n_{x^2-y^2} - n_{3z^2-r^2}}{n_{x^2-y^2} + n_{3z^2-r^2}}. \qquad (1)$$

III. RESULTS: UNRELAXED STRUCTURE

Table I presents our computed results for the orbital polarization. In this section we focus on the second column, giving results for unrelaxed structures in which all Ni-O and X-O bonds set equal to one half of the Ni-Ni distance of bulk LaNiO$_3$. Results from these structures highlight the chemical effect of interest here. Results for "z-relaxed" structures obtained by minimizing the energy with respect to atomic motions along the (001) (superlattice) direction and for structures with additional in-plane strain are discussed in Sec. V.

The calculated polarizations are seen to vary strongly with choice of counterion X. The polarization differences can also be seen directly in Fig. 2, for example, as an X-dependent change in the $d_{3z^2-r^2}$ density of states in the lower portion of

TABLE I. Orbital polarization calculated as defined in Eq. (1) for three superlattice families: "unrelaxed LNO," with all Ni-O and X-O bond lengths set equal to the GGA-optimized pseudocubic LaNiO$_3$ value of 1.905 Å; "z-relaxed LNO," with in-plane Ni-O and X-O bonds set equal to 1.905 Å and out-of-plane bonds relaxed to minimize the GGA band theory energy and "relaxed STO" in which the in-plane Ni-O and X-O bonds are set equal to 1.95 Å and out-of-plane bond lengths are relaxed to minimize the GGA band-theory energy.

X	$P_{unrelaxed}^{LNO}$	$P_{relaxed}^{LNO}$	$P_{relaxed}^{STO}$
B	0.15	−0.19	−0.10
Al	0.25	0.30	0.40
Ga	0.26	0.33	0.42
In	0.36	0.41	0.57

the antibonding band (indicated by arrow). We stress that the polarization differences occur even though all Ni-O and X-O bond lengths are equal; thus the difference is a chemical effect. We also stress that while the magnitude of the polarization depends on calculational details such as the sphere sizes and the range over which one integrates, the trends between materials are robust and clearly demonstrate that a nonstructural difference between the different X ions strongly influences the orbital polarization.

We believe that this nonstructural difference is related to the properties of a near Fermi-level orbital on the X site. To investigate this hypothesis we computed orbitally projected densities of states for the different systems. We found the most significant effect comes from the s-symmetry orbital on the counterlayer X site. In Fig. 4 we present the s projected density of states on the X site, along with the Ni $3z^2-r^2$ and apical oxygen p_z projected densities of states. Examination of the series B, Ga, and In indicates a clear correlation between the orbital polarization and the energy of the X-site s-symmetry orbital and its hybridization with the apical oxygen orbital. The Al case is an outlier in this series, for reasons not yet understood.

Higher-orbital polarization (In case) is associated with an s orbital which is farther removed in energy and less strongly admixed with O_{p_z}. Higher-orbital polarization is also associated with stronger mixing between the Ni $3z^2-r^2$ orbital and the apical O_{p_z}. Lower-orbital polarization (B case) is associated with an s orbital which is closer to the Fermi level in energy and more strongly admixed with O_{p_z} and is also associated with weaker mixing between the $d_{3z^2-r^2}$ and the apical O.

Our finding of a key role played by the s orbital on the X site is reminiscent of results of Andersen and collaborators.[18] These authors argued that in the high-T_c cuprate case the variation in the fermiology across different subfamilies of cuprate materials was controlled by the energy of the Cu $4s$ orbital, which affected the ratio of first- and second-nearest-neighbor hopping t'/t (similar arguments relating the fermiology of orbitally polarized nickelate heterostructures to the Ni $3z^2-r^2$ orbital were made by Chaloupka and Khalliulin[9]). Here we argue in an analogous way that the variation in the energy of the X-site s orbital controls the polarization of the
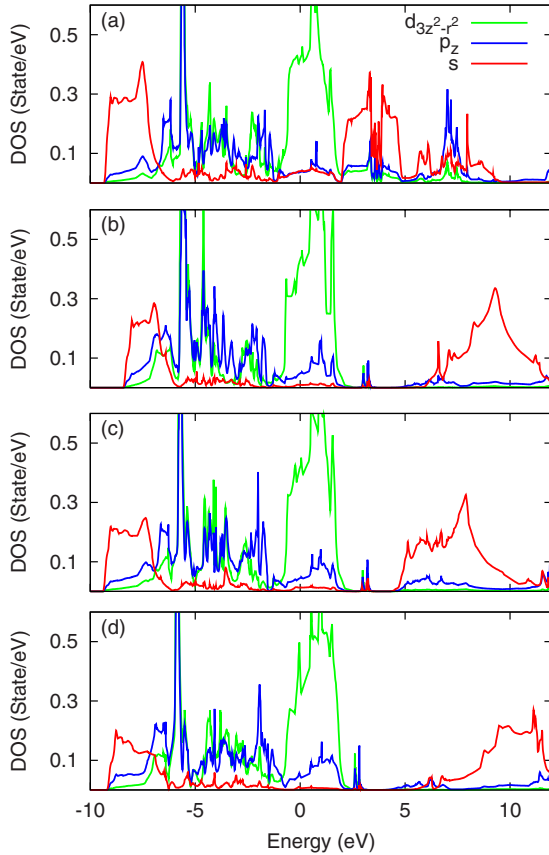
FIG. 4. (Color online) Orbital symmetry-projected densities of states for unrelaxed La$_2$NiXO$_6$ heterostructures with X=B (top panel), Al (second from top), Ga (third from top), and In (bottom). Shown are the $3z^2-r^2$ orbital on the Ni (green trace), the p_z orbital on the apical oxygen (blue trace) and the s orbital on the X site (red trace).

FIG. 5. (Color online) Density of states computed from tight-binding model projected onto Ni $d_{3z^2-r^2}$, apical O$_{p_z}$, and X_s states.

Ni d orbitals. (We also investigated the Ni 4s orbital, finding that its energy does not vary significantly across the series.)

We suggest that the polarization differences are due ultimately to changes in the hybridization between the transition-metal ion and the nearby oxygen orbitals. In the La$_2$NiXO$_6$ systems the crucial role is played by the apical oxygen which as can be seen from Fig. 1 connects the s and Ni and couples to the Ni $3z^2-r^2$ orbital but not the x^2-y^2 orbital. Fig. 4 shows that the different choices for ion X have states with differing overlap with the p_z state on the apical oxygen. Thus in essence the counterion affects the polarization by shifting the properties of the apical oxygen p_z state.

IV. TIGHT-BINDING ANALYSIS

To confirm the hypothesis that the trends reported in Fig. 4 are causally related to the observed polarization changes we turn to a tight-binding model which, while necessarily a simplified description of the actual band structure, captures with reasonable fidelity the essential features of the density of states. The specifics of the tight-binding model are given in the Appendix. We present here the main ideas. We begin with a five-band model of cubic LaNiO$_3$ consisting of the
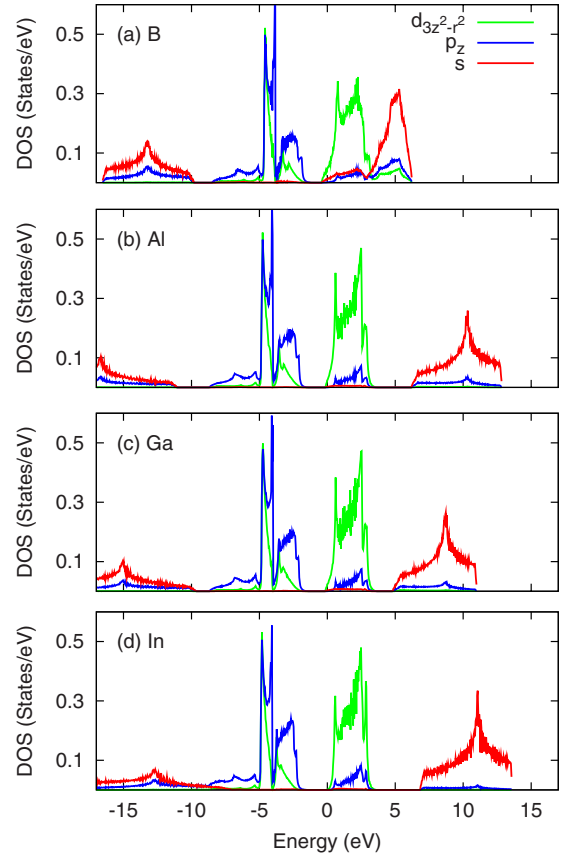
two e_g symmetry Ni d orbitals and the three oxygen p_σ orbitals. We find that a very good representation of the GGA-calculated Ni e_g and O$_{p\sigma}$ density of states for cubic LaNiO$_3$ is obtained with a Ni d-level energy of -1.22 eV, an oxygen energy of -5.2 eV, and Ni-O and O-O hopping amplitudes of 1.8 eV and 0.7 eV, respectively. We next double the unit cell in the z direction and replace one of the two Ni with an X orbital. We must then introduce three new tight-binding parameters: an energy ε_X of the orbital on the X site and hopping parameters t_{SP}, t_{SPZ} coupling the X orbital to the oxygen ions in the X plane and to the apical oxygen. The parameters ε_X, t_{SP}, and t_{SPZ} are numerically optimized by minimizing the difference between the GGA and TB densities of states of Ni$_{3z^2-r^2}$, apical O$_{pz}$ and X_S in the near Fermi level and positive energy regions. Results are shown in Fig. 5. We see that the tight-binding model reproduces the behavior of the near Fermi-level states well. Differences (for example an overestimate of the width of the low-energy $E \sim -12$ eV portion of the s band and an underestimate of the width of the high-energy $E \sim 8$ eV portion) are present but total number of X s states in the lower and upper energy portions agree well with the GGA calculations (see Appendix).

The orbital polarizations were then computed from the tight-binding model with the results P_B=0.19, P_{Al}=0.28, P_{Ga}=0.31, and P_{In}=0.39. Comparison to the information presented in Table I shows that the tight-binding polarizations reproduce well the trends found in the GGA calcula-

TABLE II. Bond lengths between Ni and apical oxygen and between X-site atom and apical oxygen presented as ratio of computed bond length to LaNiO$_3$ value $a=3.81$ Å for relaxed structures with in-plane lattice constant set to LaNiO$_3$ value (LNO) and to SrTiO$_3$ value $a=3.905$ (STO).

X	$d_{LNO}^{Ni\text{-}O}$	$d_{LNO}^{X\text{-}O}$	$d_{STO}^{Ni\text{-}O}$	$d_{STO}^{X\text{-}O}$
B	1.07	0.85	1.05	0.80
Al	1.00	1.00	0.99	0.98
Ga	1.00	1.06	0.99	1.05
In	0.99	1.19	0.97	1.16

tion. Because the only "moving part" in the tight-binding model is the X orbital the successful fitting confirms that the variation in orbital polarization between materials is in fact due to changes in nominally unfilled orbitals on the X site.

V. EFFECT OF STRUCTURAL RELAXATIONS

We finally consider the interplay of structural relaxations with the effects we have studied so far in this paper. We performed a structural relaxation process in which atoms were allowed to move in the direction transverse to the plane so as to minimize the GGA energy with the in-plane lattice constants kept equal to the bulk LaNiO$_3$ value. Table II presents the Ni-apical O and X-apical O bond lengths found after relaxation. Note that the Ni-apical O bond length is remarkably robust: almost all of the bond length change due to relaxation occurs in the X-O bond. We take this as further confirmation of the "chemical effect:" the geometrical Ni-O distance is less important than what happens at the other end of the Ni-O-X bond. The corresponding polarizations are given in the third column of Table I. Relaxation has a large effect on P, and acts to enhance the "chemical" effects we have identified. Note, in particular, that the sign of the polarization actually reverses in the B case.

The first and third panels of Fig. 6 show the GGA densities of states of the two extreme cases (B and In) computed for the relaxed structure. Comparison to Fig. 4 shows that in the boron case the X_S density of states shifts upward in energy while in the In case the X_S density of states shifts downward in energy, as expected if the position of the X orbital is controlled by hybridization with the oxygen p_z.

To show how the effects of structural relaxations are incorporated within the tight-binding model we have used the same TB parameters as in the unrelaxed case, except that we have increased t_{SPZ} in the B case (modeling the effect of a decreased X-O distance and decreased it in the In case (modeling the effect of an increased X-O distance. The resulting tight-binding densities of states are also shown in Fig. 6. The tight-binding model reproduces the basic shifts in the X-orbital density of states and leads to polarizations, $P_B^{TB}=0.08$ and $P_{In}^{TB}=0.44$.

Finally, to study the effects of in-plane strain (induced, for example, by growing on a different substrate) we set the in-plane lattice constant equal to the value 3.91 Å appropriate to the widely used SrTiO$_3$ substrate material. This corre-
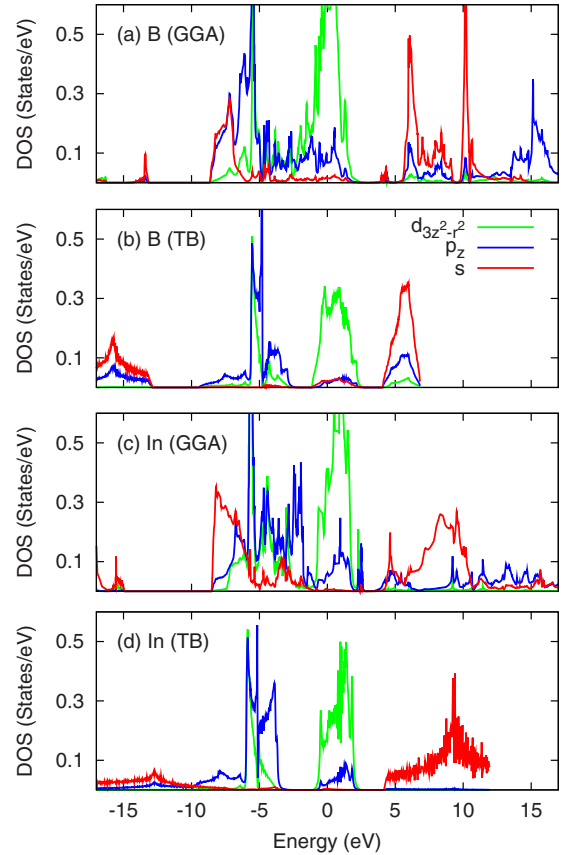

FIG. 6. (Color online) GGA orbital symmetry-projected densities of states for relaxed La$_2$NiXO$_6$ heterostructures with $X=$B (top panel) and In (third from top), along with tight-binding fits for the two cases (second and fourth panels from the top). Shown are the $3z^2-r^2$ orbital on the Ni (green trace), the p_z orbital on the apical oxygen (blue trace), and the s orbital on the X site (red trace).

sponds to applying a tensile in-plane strain. Results for the polarization are shown in the fourth column of Table I and for the lattice constants in the fourth and fifth columns of Table II. The tensile strain affects the polarization in the expected way but the out-of-plane lattice constant is again remarkably robust.

VI. CONCLUSION

Thus in summary we have shown that in addition to the well-established geometrical effect, orbital polarization in an oxide heterostructure may be controlled by appropriate choice of counterions in the superlattice. Changes in the counterion produced large orbital polarization differences, which are expected to be further enhanced by correlation effects (not yet included in our calculations). Both the magnitude and (after relaxation) the sign of the polarization can be changed. The crucial factor was found to be the hybridization of an s-like orbital on the counterion with the p_z orbital on the apical oxygen. This hybridization changed the interaction of the apical oxygen p_z with the transition-metal ion, and hence changed the orbital polarization. We also found that under structural relaxation the Ni-O bond lengths

change relatively little while the X-O bonds changed substantially. Our results thus show that the transition-metal/oxygen bond length is not the only variable controlling polarization, and that chemical effects should in general be considered when attempting to optimize superlattice properties. We remark that the need to include the s orbital demonstrates a limitation of the common theoretical strategy of deriving from band structure a "minimal low-energy model" of the system of interest. While of course a careful downfolding, keeping track of the effects stemming from bands that are projected out, will produce a low-energy model which contains the effects of interest (see, e.g., Refs. 18 and 19), construction of "minimal high-energy models" such as the one we have defined may also be a useful strategy.

APPENDIX: DETAILS OF TIGHT-BINDING MODEL

The tight-binding model presented in the text is based on the minimal assumption of a cubic ABO_3 perovskite structure with the unit cell doubled in the (001) direction and the two B sites distinguished. It involves nine orbitals: Ni x^2-y^2 and $3z^2-r^2$, the $O_{p\sigma}$ orbitals in the Ni-O plane $(O_{Ni,x}, O_{Ni,y})$, $O_{p\sigma}$ orbitals $(O_{ap1,z}, O_{ap2,z})$ at the two apical oxygen sites, an s orbital and two $O_{p\sigma}$ orbitals in the X-O plane $(O_{X,x}, O_{X,y})$.

Ordering the basis states as $(3z^2-r^2, x^2-y^2, O_{Ni,x}, O_{Ni,y}, O_{ap1,z}, O_{X,x}, O_{X,y}, O_{ap2,z}, X)$ we may write the tight-binding Hamiltonian H_{TB} in a schematic block-diagonal form as

$$H_{TB} = \begin{pmatrix} H_{Ni} & H_{pd}^\dagger & 0 \\ H_{pd} & H_O & H_{PX}^\dagger \\ 0 & H_{PX} & H_X \end{pmatrix}. \quad (A1)$$

We took $H_{Ni} = \varepsilon_d \mathbf{I}_2$ with I the 2×2 unit matrix and $\varepsilon_d = -1.22$ eV.

For the oxygen portion H_O we assumed the usual overlaps between orbitals on second neighbor oxygen, wrote the form appropriate for a simple cubic lattice, and then doubled the unit cell along (001). To avoid a cumbersome display of 6×6 matrices we write the result before doubling as

$$H_p = \varepsilon_P \mathbf{I}_3 - t_{PP} \begin{pmatrix} 0 & (1-e^{ik_x})(1-e^{-ik_y}) & (1-e^{ik_x})(1-e^{-ik_z}) \\ (1-e^{-ik_x})(1-e^{ik_y}) & 0 & (1-e^{ik_y})(1-e^{-ik_z}) \\ (1-e^{-ik_x})(1-e^{ik_z}) & (1-e^{ik_z})(1-e^{-ik_y}) & 0 \end{pmatrix}. \quad (A2)$$

Here $\mathbf{I}_3$ is the 3×3 unit matrix and we took $\varepsilon_P = -5.2$ eV and $t_{PP} = 0.7$ eV. Inclusion of oxygen-oxygen hopping is necessary to reproduce the narrow d feature observed at $E \sim -6$ eV in, e.g., Fig. 2 of the main text. H_O is just H_P doubled in the z direction.

For the p-d hopping we took the standard form

$$H_{pd} = -t_{pd} \begin{pmatrix} \frac{1}{2}(1-e^{ik_x}) & -\frac{\sqrt{3}}{2}(1-e^{ik_x}) \\ \frac{1}{2}(1-e^{ik_y}) & \frac{\sqrt{3}}{2}(1-e^{ik_y}) \\ -e^{-ik_z/2} & 0 \\ 0 & 0 \\ 0 & 0 \\ e^{i(k_z/2)} & 0 \end{pmatrix} \quad (A3)$$

with $t_{pd} = 1.8$ eV while for H_{XP} we put

$$H_{PX} = \begin{pmatrix} 0 \\ 0 \\ -t_{SPZ}e^{ik_z/2} \\ t_{SP}(1-e^{-ik_x}) \\ t_{SP}(1-e^{-ik_y}) \\ t_{SPZ}e^{-ik_z/2} \end{pmatrix}. \quad (A4)$$

The important parameter is t_{SPZ} giving the overlap between the s orbital and the apical oxygen states.

The tight-binding parameters are not uniquely determined; changes in one parameter may be to some extent

TABLE III. Tight-binding parameters used to construct fits displayed in Fig. 4 of main text with resulting orbital polarization.

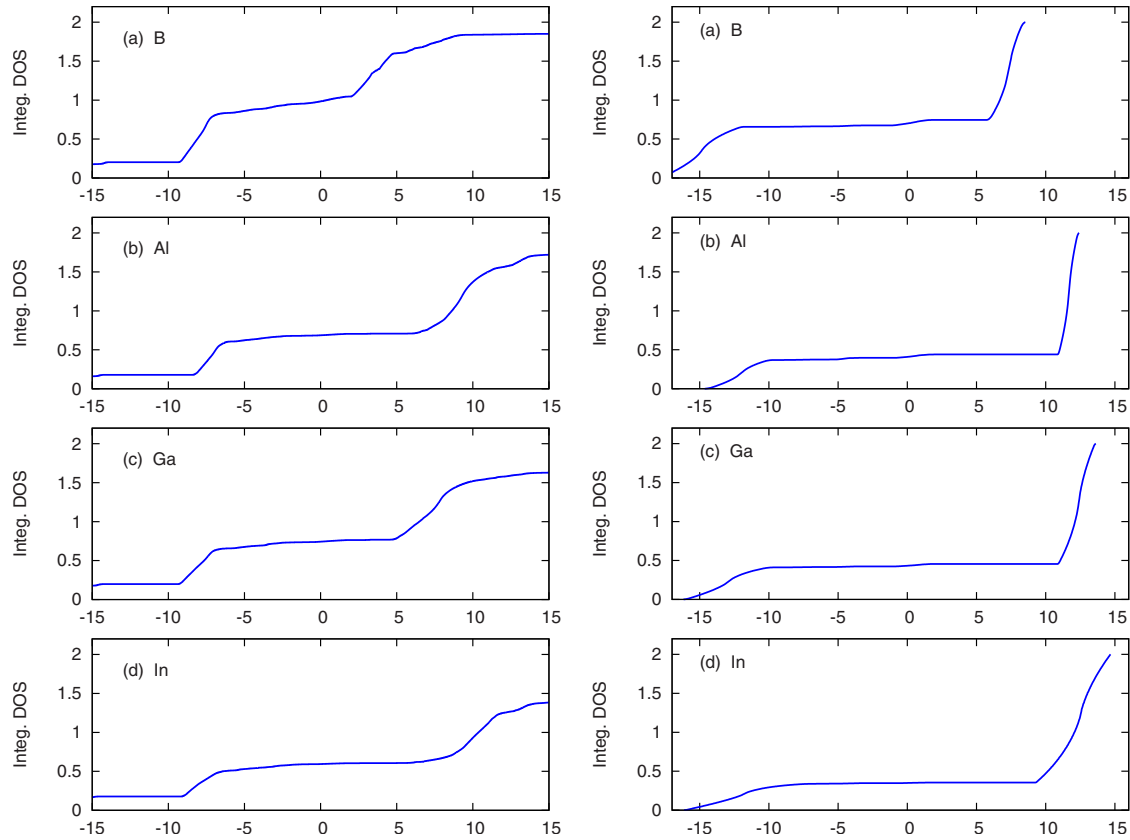|	t_{SP}	t_{SPZ}	ε_X	P
B	3.0	4.5	−4.0	0.19
Al	5.0	6.0	−1.6	0.28
Ga	4.5	5.0	−1.6	0.31
In	4.5	4.0	3.2	0.39

FIG. 7. (Color online) Left panel: integral of $X\,s$ GGA density of states for the four choices of X ion considered in the paper. Right panel: integral of $X\,s$ TB density of states for the four choices of X ion considered in the paper.

compensated by changes in another, but as long as the density of states and s-apical p_z mixing are reproduced with reasonable accuracy the polarization is robust. We chose to fix the tight-binding model parameters by first choosing the Ni-related parameters to fit the GGA band structure of cubic LaNiO$_3$. Then we determined the other orbitals by minimizing the "distance" between the GGA and TB predictions for the density of states of the $3z^2-r^2$, O p_z, and X_S orbitals. That is, we chose the TB parameter set which minimizes $\Sigma_{\mathcal{O}} \int d\epsilon [\rho(\epsilon)_{\mathrm{GGA}}^{\mathcal{O}} - \rho(\epsilon)_{\mathrm{TB}}^{\mathcal{O}}]^2$, where $\rho(\epsilon)^{\mathcal{O}}$ denotes the density of states for orbital $\mathcal{O}=$Ni $d_{3z^2-r^2}$, O_{pz}, or X_S atom and the energy ranges are -1 to 2 for the Ni, -10 to the upper limit for the O_{pz}, and -2 to the upper limit X_S orbitals. The parameters used to produce the fits shown in the text for the unrelaxed structures are summarized in Table III along with the resulting polarizations. To model the

effects of structural relaxation in the In case we decreased the t_{SPZ} from 4 to 2.5 and in the B case we increased it from 4.5 to 6. The resulting polarizations are $P_{\mathrm{B}}^{\mathrm{TB}}=0.08$ and $P_{\mathrm{In}}^{\mathrm{TB}}=0.44$.

Figure 7 compares the integrated $X\,s$ density of states obtained from GGA and optimized TB calculations, respectively. Some differences are visible. At the very low end of the energy range ($E \sim -8$ to -12 eV the X density of states extends to low energies in the tight-binding model than it does in the GGA calculation, presumably because of level repulsion arising from other low-energy orbitals present in the GGA calculations but not in the tight-binding model. Similarly, at the very high end of the range the tight-binding model underestimates the width of the S band but these differences do not affect the qualitative conclusions we wish to draw.

[1] J. Mannhart, D. A. Blank, H. Y. Hwang, A. J. Millis, and J. M. Triscone, MRS Bull. **33**, 1027 (2008).

[2] K.-I. Kobayashi, T. Kimura, H. Sawada, K. Terakura, and Y. Tokura, Nature (London) **395**, 677 (1998).

[3] U. Lüders, W. C. Sheets, A. David, W. Prellier, and R. Frésard, Phys. Rev. B **80**, 241102(R) (2009).

[4] S. Jin, T. Tiefel, M. McCormack, R. A. Fastnacht, R. Ramesh, and L. Chen, Science **264**, 413 (1994).

[5] M. Imada, A. Fujimori, and Y. Tokura, Rev. Mod. Phys. **70**, 1039 (1998).

[6] J. Bednorz and K. Muller, Z. Phys. B: Condens. Matter **64**, 189 (1986).

[7] Y. Tokura and N. Nagaosa, Science **288**, 462 (2000).

[8] Y. Konishi, Z. Fang, M. Izumi, T. Manako, M. Kasai, H. Kuwa-

hara, M. Kawasaki, K. Terakura, and Y. Tokura, J. Phys. Soc. Jpn. **68**, 3790 (1999).

[9] J. Chaloupka and G. Khaliullin, Phys. Rev. Lett. **100**, 016404 (2008).

[10] P. Hansmann, X. Yang, A. Toschi, G. Khaliullin, O. K. Andersen, and K. Held, Phys. Rev. Lett. **103**, 016401 (2009).

[11] E. Ruiz-Trejo, G. Tavizon, and A. Arroyo-Landeros, J. Phys. Chem. Solids **64**, 515 (2003).

[12] J. Fan, Z. Lin, L. Zhang, and G. Wang, J. Phys. D: Appl. Phys. **39**, 3226 (2006).

[13] G. Kresse and J. Hafner, Phys. Rev. B **47**, 558 (1993).

[14] G. Kresse and J. Hafner, Phys. Rev. B **49**, 14251 (1994).

[15] G. Kresse and J. Furthmuller, Comput. Mater. Sci. **6**, 15 (1996).

[16] G. Kresse and J. Furthmuller, Phys. Rev. B **54**, 11169 (1996).

[17] G. Kresse and D. Joubert, Phys. Rev. B **59**, 1758 (1999).

[18] E. Pavarini, I. Dasgupta, T. Saha-Dasgupta, O. Jepsen, and O. K. Andersen, Phys. Rev. Lett. **87**, 047003 (2001).

[19] O. K. Andersen, A. I. Liechtenstein, O. Jepsen, and F. Paulsen, J. Phys. Chem. Solids **56**, 1573 (1995).